



Effect of hard and soft re-coater blade on porosity and processability of thin walls and overhangs in laser powder bed fusion additive manufacturing

Joni Reijonen^{1,2} · Alejandro Revuelta¹ · Sini Metsä-Kortelainen¹ · Antti Salminen²

Received: 23 May 2023 / Accepted: 10 December 2023 / Published online: 15 December 2023
© The Author(s) 2023

Abstract

Spreading powder into thin layers is a fundamental step in the laser powder bed fusion (PBF-LB) additive manufacturing process. This step is called re-coating and it is typically performed using either a hard, soft or brush-type re-coater blade or a rotating roller, depending on the machine brand and model. With such variety in powder spreading approaches, the question arises whether the used re-coater type has a significant effect on the quality of parts produced? In this study, an industrial contact image sensor integrated to the re-coater of a PBF-LB system was used for powder bed quality monitoring. Powder bed images at 21 μm /pixel resolution, 184 mm scanning width and 95 mm/s re-coating speed were acquired. With this, the effect of using either soft (rubber) or hard (steel) re-coater blade on the processability of challenging features such as thin walls and steep overhangs was studied. In addition, porosity and dimensional accuracy of parts produced using either the soft or hard blade was analyzed with X-ray computed tomography. It is shown that when building bulk material without any complex features, both the hard and soft re-coating blade results in extremely low porosity $\leq 0.001\%$ without any issues in the processability. However, when thin walls and overhangs are produced, differences in processability, porosity and dimensional accuracy are observed as a function of re-coater blade and part orientation. This is an important factor in understanding all the significant sources contributing to the variability on quality of parts produced using different PBF-LB machines.

Keywords 316L · Computed x-ray tomography · Contact image sensor · Laser powder bed fusion · Re-coating · Quality

1 Introduction

In laser powder bed fusion (PBF-LB) additive manufacturing (AM), one of the fundamental elements in the build cycle is the application of the metal powder into thin layers, usually in layer thicknesses of 20–100 μm [1–4]. This processing step is called re-coating and it is typically performed using either a hard, soft or brush-type re-coater blade or a rotating roller, depending on the machine brand and model [1, 5]. Some machine models have a fixed re-coater design, while in others the operator may choose which type of blade to use. Furthermore, the fresh powder is supplied either from

a bin below the processing plane or using a hopper feeding the powder from above. Various blade tip geometries from extremely sharp to filleted and from flat to round are utilized in re-coating blades. With such variety in powder spreading approaches, the question arises whether the used re-coater type has a significant effect on the quality of the spread powder layer and in the end, on the quality of parts produced. From qualification perspective, should the re-coater blade type be considered an essential parameter in the PBF-LB process? The need for further research on the effect of powder spreading approach to the final part properties was also highlighted in a recent comprehensive review by Capozzi et al. [1] on powder spreading in AM.

In the past, multiple studies have been conducted to analyze the powder bed characteristics with different re-coating strategies, without extending the study to the finished part properties. Jacob et al. [6] developed an offline method to measure the effective powder bed density printing hollow canisters that trap powder in a measurable volume during the printing, which is then measured post print. Similar

✉ Joni Reijonen
joni.reijonen@vtt.fi

¹ VTT Technical Research Centre of Finland Ltd, Advanced Manufacturing Technologies, 02044 Espoo, Finland

² Department of Mechanical and Materials Engineering, University of Turku, 20014 Turku, Finland

approaches were used by Choi et al. [7] and Wischeropp et al. [8]. Oropeza et al. [9] used transmission x-ray imaging to study the effect of powder and re-coating parameters on the spread powder layer density. Marchais et al. [10] and Shaheen et al. [11] conducted simulation studies utilizing the discrete element method (DEM) to study the effect of powder characteristics and spreading parameters on the properties of the powder bed. Haeri [12] and Wang et al. [13] further used DEM simulations to study the effect of the re-coater geometry on powder bed properties. Various other DEM simulation studies on powder spreading in PBF-LB have been conducted, summarized recently in a review paper by Li et al. [14]. Such DEM studies do not provide any indication whether these differences observed in the simulation when using different re-coater blade types are severe enough to result in observable variability in quality of parts produced. Oropeza et al. [15] and Hulme et al. [16], among others, have developed custom built powder spreading test beds to experimentally analyze powder spreading and develop quality metrics for the spread powder layer. Utilizing such test beds, Snow et al. [17] used video and optical images whereas Yuasa et al. [18] used fringe projection to analyze powder bed properties. Such test beds can be used to study the effects of powder and re-coating parameters on the powder layer quality, but lack the ability to study whether this has an effect on the final part properties in PBF-LB as no laser melting takes place.

In addition to potentially forming defects that may go undetected during the production stage and deteriorate the quality of the finished material, the choice of the re-coater blade affects the failure or success of the build altogether. Daña et al. [19] reported that the use of a hard (in their case ceramic) re-coater blade is less suited for thin features such as many support structure types commonly used in PBF-LB AM as the contact of a thin feature with a hard re-coater is prone to deform the thin features and disturb the powder bed around the feature in the process. Furthermore, it is well-known that a collision with a part/feature that has risen above the powder bed with a hard re-coater may cause the re-coater to jam or even break, stopping the build, resulting in production downtime. On the other hand, a similar collision while using a soft re-coater blade may damage the blade, which will lead to the formation of scratches (resulting in local variation in the effective powder layer thickness) on subsequent layers after the collision.

Recently, some studies have been conducted that indicate that the re-coater blade type has an effect on the final part properties. Shamsdini et al. [20] has studied the use of a ceramic and carbon fiber brush-type re-coater blades in PBF-LB. In their study, using 18-Ni300 maraging steel powder, the elongation at fracture was significantly lower in the specimens manufactured with the carbon fiber brush. The fractography revealed the presence of unmelted particles

in those specimens, indicating lack-of-fusion defects. The results of their study indicated that the type of re-coater blade used may have an influence on mechanical properties in PBF-LB. More recently, Fox et al. [5] studied the effect of the re-coater blade on mechanical properties of Ti-6Al-4 V parts produced in PBF-LB. They produced identical sets of test specimens using steel, rubber and carbon fiber brush re-coater blades. The number of tensile test specimens in their study was quite significant ($N=36$) and they concluded there was no significant difference in tensile strength regardless of blade used. Unfortunately, they did not report anything on tensile elongation. However, they noticed that parts produced using the soft blades (rubber or brush) had overall higher pore density and larger pores than parts made with the hard steel blade. This could indicate reduced elongation and fatigue performance, for which porosity is a good indicator [21].

Another branch of research focuses on online quality monitoring of the powder bed at each layer. A common approach that is also commercially available from some PBF-LB machine manufacturers is to acquire images with an optical camera mounted off-axis in relation to the powder bed. The main challenges with this method are related to obtaining undistorted images at sufficiently high resolutions from the entire build area with uniform illumination at all locations. Abdelrahman et al. [22] used this method for flaw detection from the surfaces of parts being produced. The achievable pixel resolutions were around 40–90 μm , depending on the distance from the camera to a given location on the build area. Lu et al. [23] used a camera mounted outside the build chamber to acquire the images via a mirror placed above the build area and with considerable effort on achieving uniform lighting by adding additional LEDs to provide light from various sides of the build area. They were able to establish correlations between laser parameters and features extracted from the acquired images on laser melted part surfaces. To have co-axial view, Barrett et al. [24] used laser profilometer mounted to the re-coating arm and Fleming et al. [25] used in-line coherent imaging placed at the optical arrangement of the PBF-LB system to monitor the laser melted surface profiles.

To increase resolution, to have consistent illumination conditions and distortion free images directly from above the powder bed, line cameras mounted directly to the re-coater provide a promising method. Fischer et al. [26] utilized a line camera integrated on the re-coater of a PBF-LB system to acquire images of the powder bed at a combined high resolution (5.97 $\mu\text{m}/\text{px}$) and practically relevant re-coater speed of 100 mm/s. Their study focused on analyzing the melted layer quality from the acquired images and identifying defects as a function of laser parameters while keeping the re-coating scheme constant. In their recent paper, they used the images acquired to train neural networks to identify

defects in the spread powder layers [27]. Pedersen et al. [28] proposed the use of a contact image sensor (CIS) from an office flatbed scanner for optical monitoring of the powder bed quality. Tan Phuc and Seita [29] and Le et al. [30] built upon this and performed comprehensive studies and developed image analysis schemes to derive quality metrics for the spread powder layer based on the images acquired via a CIS. Based on the developed metrics, they compared the powder layer properties when using a rubber or steel re-coater blade for the spreading and showed that there are differences within many of the used metrics. In their most recent publication, they were able to produce $\varnothing 5$ mm and 5-mm-tall cylindrical samples and establish correlations between different laser processing conditions and part density via the laser melted surface appearance as imaged with the CIS [31]. The CIS images were acquired in colour at 1200 dpi resolution and it was reported to take ~ 1 min for imaging each layer, due to the low image acquisition frequency of the used consumer grade CIS. Elsewhere, Bugatti and Colosimo [32] also recently reported early studies on integrating CIS to monitor the powder bed and showed that the images acquired provided much higher resolution and enhanced ability to discern relevant features than an off-axis camera. Most recently, Hui et al. [33] used a high speed CIS integrated on a bi-directional re-coater in PBF-LB system to acquire layer-wise images with 1200 dpi resolution and 95 mm/s speed (less than 2 s per imaged layer) for multi-scale image analysis using wavelet transformation and established correlations with laser melted surface features viewed at multiple scales to the built part density.

In this study, an industrial CIS (intended for bank note counting) integrated to the re-coater of a PBF-LB system was used for powder bed quality monitoring. This setup allows for the acquisition of monochrome images from the powder bed at a resolution of 1200 dpi (21 $\mu\text{m}/\text{pixel}$), 184 mm scanning width and with 95 mm/s re-coating speed. With this, the effect of using either soft (rubber) or hard (HSS) blade on the processability of challenging features such as thin walls and steep overhangs was studied. In addition, porosity and dimensional accuracy of parts produced using either the soft or hard blade was analyzed with X-ray computed tomography (CT).

2 Materials and methods

SLM 125 HL PBF-LB system from SLM Solutions GmbH was used to conduct the experiments. The laser wavelength was 1070 nm and the focal point diameter 80 ± 6 μm . Argon was used as shielding gas and the shielding gas flow speed was 7.0 m/s at the inlet piping as set from the machine control program. The oxygen content in the build chamber was < 1000 ppm during the experiments. Standard set

of laser processing parameters developed by the machine manufacturer for 316L material using layer thickness of 30 μm was used. The scanning strategy proceeds by first making two border vectors, then an infill vector and finally the core vectors. The main laser parameters for core vectors were 200 W for power, 800 mm/s for scanning speed and 0.12 mm for hatch distance. The core hatching vectors are rotated between layers, having a starting angle of 5° and a subsequent rotation of 33° as illustrated in Fig. 1b. On the platform scale, the scanning sequence is from left to right (against shielding gas flow) in Fig. 1a. Re-coating speed was set to 95 mm/s (down from the typical 215 mm/s in the SLM 125 system) as required by the CIS to obtain undistorted images at the full 1200 dpi resolution. No additional building platform pre-heating was applied.

The build included three specimens with a set of thin walls (wall thickness 2.0, 1.5, 1.0, 0.7, 0.5 and 0.3 mm) placed at different angles (0° , 45° and 90°) in relation to the re-coater and two specimens with a set of overhangs (inclined 45° , 40° , 35° , 30° and 25° relative to the building platform) placed perpendicular and along the re-coating direction. The build layout is shown in Fig. 1a and the specimen dimensions in Fig. 1c and d. The specimens were placed on the build platform in their own re-coating sectors indicated by the dashed lines to ensure that collision and subsequent possible re-coater damage with one specimen would not affect the other specimens. All specimens were manufactured directly onto stainless steel platform, meaning that 2 mm from the 6 mm bottom of all specimens were allowance for separating the parts after the build from the platform with a band saw. Support structures were not used on the overhangs or thin walls with the purpose of inducing easily observable responses in the case of differences in regard to the re-coater blade used. Furthermore, it is preferable and in some designs even necessary to avoid the use of support structures due to challenges in their removal, for example in internal structures that are not open to the surface of the part. No post-process heat treatment nor surface treatments were applied and the specimens were used for further analysis in as-built condition.

Gas atomized 316L stainless steel powder from Carpenter Additive was used. Figure 2 shows the relevant characteristics of the powder, namely particle size distribution measured with laser diffraction particle size analyser Malvern Mastersizer 3000, morphology imaged with scanning electron microscope JEOL JSM-636OLV and chemical composition measured with LECO ONH-836 for O, N and H, LECO CS 744 for C and S and Thermo-Fischer iCAP7400 Duo for the other elements.

Two identical builds were produced with the re-coater blade as the only variable, while other process parameters were kept constant. Two different re-coater blades (soft and hard) with different blade tip profiles were used. The soft

re-coater blade used was the standard polymer composite re-coater blade used in the SLM 125 HL machine. The hard re-coater blade was the standard high speed steel blade used in EOS M290 machine. The blade tip profiles are shown in Fig. 3 As the re-coater (and the rubber blade) in the SLM 125 HL used for conducting the experiments is bi-directional

by design, two hard blades were installed side-by-side to enable bi-directional re-coating also with the hard blades.

The powder bed quality was monitored by using a model SWL12R183NDU-211216 CIS from Weihai Hualing Opto-Electronics Co., Ltd. (WHEC), to capture images of the powder bed after re-coating and after laser scanning. This

Fig. 1 (a) Build layout and specimen orientations, (b) scanning strategy, (c) overhang specimen geometry and (d) thin wall specimen geometry. The red circles in (a) indicate no-build zones for platform mounting screws

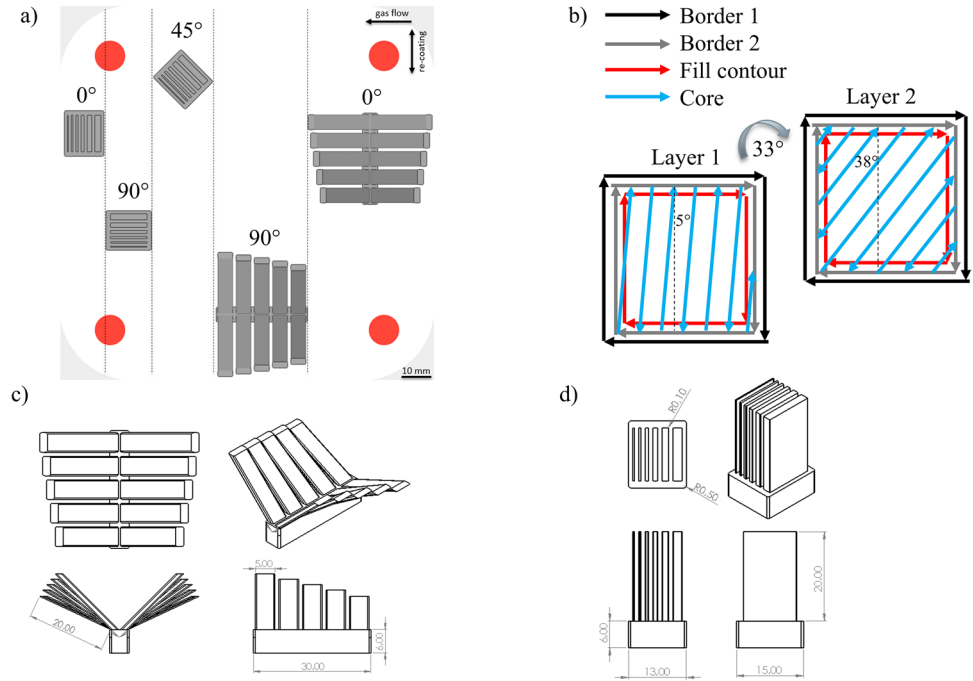


Fig. 2 (a) Particle size distribution, (b) SEM image of morphology and (c) chemical composition of the used 316L powder

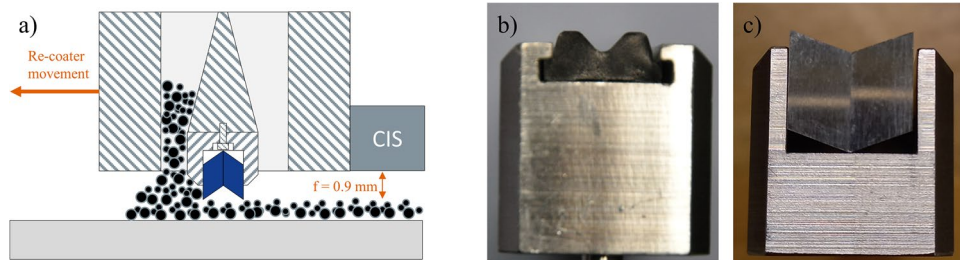
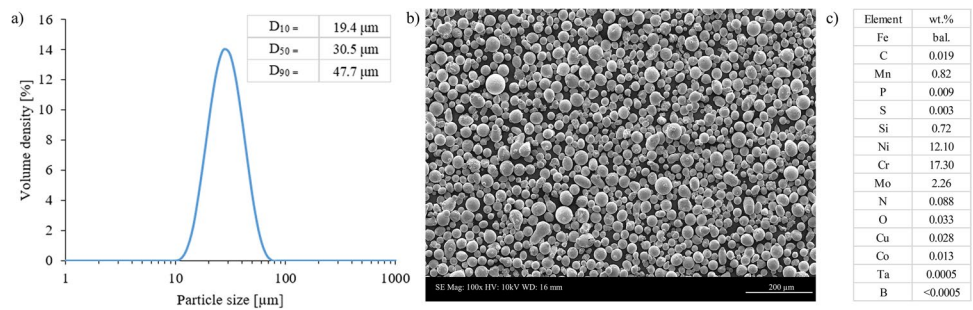


Fig. 3 (a) Simplified schematic of the bi-directional re-coater and the integrated CIS unit, (b) soft re-coater blade profile and (c) hard re-coater blade profile. Note that (a) represents a situation when

re-coater is moving from front to back (even layers) and the CIS is acquiring an image of a freshly spread powder layer

particular CIS sensor was selected as it is capable of acquiring high (1200 dpi) resolution images at industrially relevant scanning speed (95 mm/s), combined with small dimensions of length = 200 mm, width = 18 mm and height = 14 mm. Selecting a compact sensor design was necessary to be able to retrofit it to the standard re-coater unit of the SLM 125 system and not to have the sensor block parts of the active build area. The CIS was mounted on the front side of the bi-directional re-coater, meaning that an image of the laser melted powder bed would be acquired on odd layers (1, 3, 5...) and an image of re-coated powder layer on even layers (2, 4, 6...). The re-coater position was used as the triggering signal to acquire images starting right before, and ending just after, the building platform. This setup allows for the acquisition of monochrome images from the powder bed at a resolution of 1200 dpi (21 $\mu\text{m}/\text{pixel}$), 184 mm scanning width and with 95 mm/s re-coating speed.

In this study, the images from every second layer that is acquired from a freshly re-coated powder bed were utilized. The aim was on identifying any anomalies in the powder spreading and specifically on identifying areas where the powder layer height deviates from the nominal. Due to the extremely short focal depth of the used CIS, areas from which powder has been depleted and is further away from the CIS are out of focus, resulting in blurriness of the image at this location. For quantifying this phenomenon from the images, the focus level of the acquired images is calculated using a modified Laplacian focus measure operator (FMO) as described in [29]. The image processing sequence is shown in Fig. 4. First, the region of interest is cropped from the entire build area, which in this case is the 45° thin walls specimen and regions around it. Then, the FMO is calculated and the results obtained from the FMO are smoothed using a box filter. The window pixel size of the box filter used was 21. Thirdly, purely for visualization purposes, a heat map colour image is generated from the grayscale FMO images. Finally, to quantify the possible anomalies on the focus map images, the mean and standard deviation of the grey value of the whole stack of FMO images was calculated and the mean minus three times the standard deviation value was used as the threshold. Pixels with value below

the threshold, denoted as black, correspond to out of focus, whereas pixels above the threshold in white would be in focus. The share of black to white pixels is then calculated for each layer, to have a quantified value used in the results as %-share of out of focus area in the image.

From Fig. 4, one can notice, that while the out of focus (in this case further away from the CIS, denoted as yellow in the heat map), there is another region in darker red, that is distinguishable from the background when using the FMO. Such regions correspond to areas that are closer to the CIS (in other words, where there is excess powder) and have a higher value for the Laplacian focus measure. This means that such areas are actually more in focus than the background. This suggests that the CIS sensor was not perfectly in focus in relation to the nominal powder bed surface, but rather, the perfect focus would have been slightly higher. Nevertheless, out of focus regions of the magnitude caused by the phenomenon observed here are clearly identified by the method.

CT scanning of the specimens was conducted using GE Phoenix vltomelx s system with a 240 kV direct microfocus tube and a 1.0-mm Cu filter was used. The specimens were scanned using helical scanning to minimize artefacts. For all the thin-walled specimens, a voxel resolution of 11 μm was used and for the overhang specimens resolution was 16 or 11 μm depending on the total part size. A generic rule of thumb is that defects with a size $> 2\text{--}3$ voxels can be reliably identified. For 11- μm resolution, the scanning voltage was 200 kV and the current 58 μA . For 16- μm resolution, the scanning voltage was 200 kV and the current 85 μA . Image exposure time was 1000 ms in all samples. The 3D volumetric scan data was visualized, processed and analyzed as 8-bit TIF image stack using ImageJ software (GNU General Public Licence, version 1.53t). Porosity was analyzed from the CT scan data using the Analyse Particles function of ImageJ software. For this purpose, the image stack was thresholded to binary black and white images. First, the part outlines as a region of interest (ROI) were identified and the area calculated to get the true manufactured volume of the part or feature in question. Then, internal voids within the ROI were identified for each slice in the CT scan data.

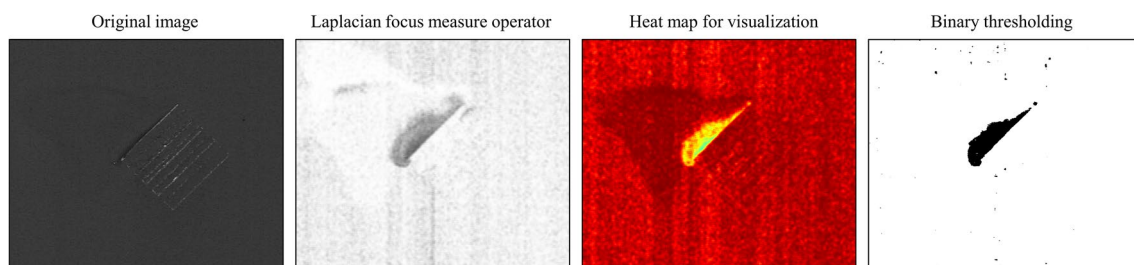


Fig. 4 Laplacian focus measure was used to identify out of focus areas on the powder bed from CIS images

Figure 5 illustrates the porosity calculation method for the CT data. Threshold was selected such as to minimize noise and to focus on identifying large ($> 1\text{px}$) defects. For the thin walls used in the porosity analysis, threshold was set to 120 (on a 0–255 pixel intensity range in 8-bit image). For the overhangs, the threshold was set to 80.

3 Results and discussion

3.1 Processability

The first assessment on the capability of both re-coater blades to process the studied features was simply to observe if the parts can be built all the way to the end of the build cycle. With the soft re-coater, the build with all the parts was finalized; however, some features rising up from the powder bed caused noticeable damage to the re-coater blade during the build. With the hard re-coater, a collision between the hard unyielding re-coater blade and a rising feature from the powder bed caused such a forceful collision, that the process had to be stopped three times to avoid damaging the re-coating system severely. First, the thin-walled specimen oriented 90° in relation to the re-coating direction collided after just ~ 15 layers of building the thin walls and had to be discontinued from the build. Next, after ~ 30 layers of building the specimen with the overhangs oriented horizontally (i.e. 90°), it collided with the re-coater and had to be discontinued for the same reason. Lastly, after ~ 100 layers of building the other overhangs, a fatal collision happened and the part had to be discontinued from the build. The remaining two thin-walled specimens (0° and 45°) were built until the end successfully.

Next, the processability of the features was analyzed from the powder bed images obtained with the CIS. Various types of powder bed disturbances could be identified from the CIS images depending on the processed geometrical feature and re-coater blade type used. Note that these images are all taken after re-coating a fresh powder layer. Figure 6

summarizes the types of anomalies observed. Two common process phenomena for PBF-LB are identified, namely spattering and features rising above the powder bed. From these phenomena, the type of disturbances to the powder bed and consequences to the part being processed are different, depending whether a soft or hard re-coater blade is used. When using soft re-coater blade, spatters landing on the part surface were observed to remain on it after re-coating (Fig. 6a). The spatters are larger than the used layer thickness of $30\ \mu\text{m}$ and can be clearly observed even after spreading a fresh powder layer. When using a hard re-coater blade, little-to-no spatters were observed on the part surfaces after re-coating. Instead, on some layers, it was clearly observed that the spatters had been shaved off the part surface, dragged along the re-coater blade and distributed to another location on the powder bed, as seen on Fig. 6d. When a feature (such as thin wall or steep overhang) starts to deform upwards from the powder bed (Fig. 6b, e), it eventually leads to collision with the re-coater blade. If a soft re-coater blade is used, often the sharp metallic feature rising from the powder bed damages the soft blade. This results in noticeable scratches to the powder bed on subsequent layers after the collision (Fig. 6c). If a hard re-coater blade is used, a similar collision with the unyielding hard blade results in damage to the feature being processed (Fig. 6f). If neither the hard re-coater blade nor the part yields, the re-coater may jam or break, stopping the build cycle. A contact between the hard re-coater blade and a thin wall that readily bends but does not break was seen to cause frequent powder bed disturbances on its vicinity (Fig. 6g). Similar powder bed disturbances were observed in [19] when processing thin support structures with a hard re-coater blade.

From these observed anomalies in the powder bed, in this study the focus was on quantifying the phenomenon shown in Fig. 6g following the method described in Sect. 2. As this phenomenon did not cause the process to stop nor results in an obvious failure of the part being built, it provides a great example of a process disturbance that could produce internal

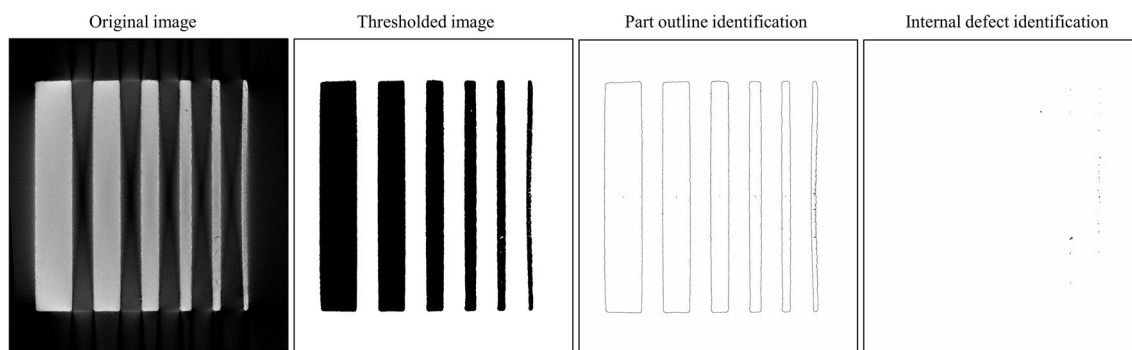


Fig. 5 Porosity calculation method from CT scan data. Here, a single 2D slice for the thin walls as imaged from above is presented. The calculation was conducted for all the 2D slices in the 3D stack

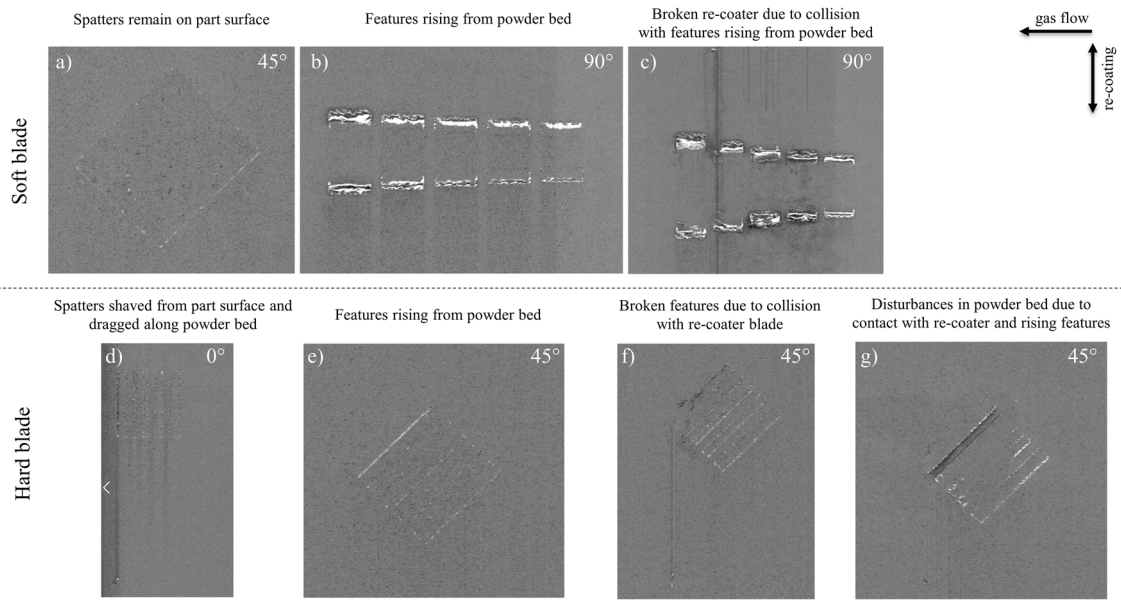


Fig. 6 Observed powder bed anomalies from the contact image sensor images, (a–c) for soft re-coater blade and (d–g) for hard re-coater blade

defects that go unnoticed in the finished part, unless such powder bed images are collected for each layer. Furthermore, this phenomenon was seen frequently when processing thin walls with the hard re-coater blade, but rarely with the soft blade; hence, it provides interesting comparison between processability with the different re-coater blades. Figure 7 shows a plot of the calculated share of out of focus area in the region of interest due to collision with the thin wall and subsequent disturbance to the powder layer height in its vicinity per layer for both the hard and soft blade. Furthermore, the Laplacian focus measure images as heat map for the value are shown from layers 50, 212 and 360 as examples from different relevant events in the build. Note that the absolute value for the background in the images (the powder bed) is different between the hard and soft re-coater builds. This is due to different absolute grey

scale values (a difference of approximately 5 in the mean of the histograms) in the original images, which could be due to many reasons, such as differences in lightning conditions between the builds. Nevertheless, this does not preclude one from distinguishing deviation, or the absence of it, from the background, which was the purpose here and which is used as the calculated value in the graph.

In Fig. 7, the first 200 layers (height of 6 mm) of the build correspond to the solid bottoms of the specimens. It can be seen, that during 1–200 layers, the percentage out of focus remains relatively low for both builds. Images from layer 50 for both the hard and soft re-coater builds are shown to illustrate that nothing can be distinguished from the background at this stage, as there are no out of focus areas. After this, the building of the thin walls begin and

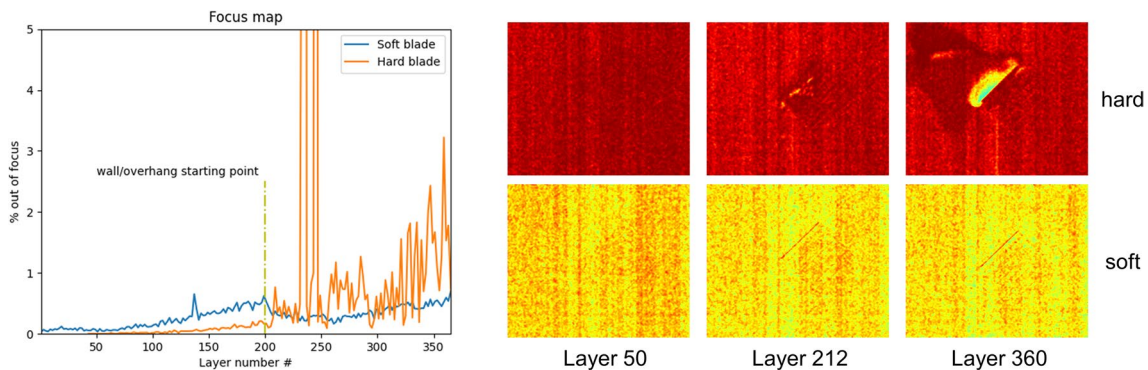


Fig. 7 Share of out of focus areas due to powder bed disturbances as a function of built layer when processing with soft and hard blade. Heat map images from the Laplacian focus measure of layers 50, 212 and 360 are included

there is change in the trend. When using the soft blade, the share of out of focus regions actually decrease after layer 200, when the building of the thin walls begins. This is due to the edges of the thin walls protruding above the powder bed surface, as can be seen in the image from layer 212 for the soft blade. As explained in Sect. 2 and seen on Fig. 4, areas that are closer to the CIS actually become more in focus than the nominal powder bed in this case, due to slight error on mounting the CIS to be perfectly in focus (distance of 0.9 mm from the CIS glass) in relation to the undisturbed powder bed. When building the thin walls (layers above 200) with the soft blade, the share of out of focus regions in the image remains low, mostly below 0.5%. When building the thin walls with the hard blade, there is a clear difference. Once the thin walls start at layer 200, just few layers after the share of out of focus regions start to increase, as illustrated for the layer 212. On layer 360, the share of out of focus area in the image is already above 3%. There is high variance between individual layers, which reflects the fact that a collision with the thin wall and the hard blade does not occur at every layer, but on some of them. An increase in the share of out of focus area is seen on those layers where there has been impact and the powder bed has been disturbed. On layers 235, 237 and 246 (high peaks that go above the scale in the graph) with the hard re-coater blade, there was a severe enough collision that the image is almost totally out of focus. This was either due to disturbance to the steady speed of the re-coater (and the attached CIS) or a jump of the re-coater and hence a shift in the working distance of the attached CIS, as a result of the impact. In these cases, the impact was severe enough that it disturbed the acquisition of the image itself, rather than reflecting only a disturbance on the powder bed.

3.2 Dimensional accuracy

In addition to the obvious shortcomings in processability leading to some features not being able to build at all as explained above, it was also studied if the choice of re-coater blade affects the accuracy of the finished features. For this purpose, the cross-sectional area of each slice in the CT images for the thin walls was extracted as shown in Fig. 5. First, the average and standard deviation along the whole wall heights were calculated, from which the metric coefficient of variation (CoV) was calculated as average divided by standard deviation ($CoV = Average / STD$). The results are plotted in Fig. 8 as a function of wall thickness, re-coater blade and part orientation. For qualitative illustration of the surface roughness and dimensional accuracy of the walls in general, the 3D surface volume created from the CT scan data of the wall features is included. Regardless of re-coater blade and part orientation, the accuracy as measured by the variation in cross-sectional area along the height decreases when the wall thickness is decreased, as could be expected. This is in good agreement with previous studies [34], the error in the dimension of relatively thick walls (above 1 mm in this case) reaching $< 0.4\%$. Going to walls thinner than 1 mm, the error in dimensional accuracy increases exponentially. However, it can be seen that the re-coater blade and part orientation together determines the severity of the loss of dimensional accuracy. In this case, worst accuracy is observed when hard re-coater blade is used and the part is in 45° angle in relation to the re-coating direction. When comparing the hard and soft re-coater blade in each part orientation, it can be seen that in all of them, the soft re-coater performed better (in 90° orientation the quantitative comparison is not valid, as the walls using hard blade in this

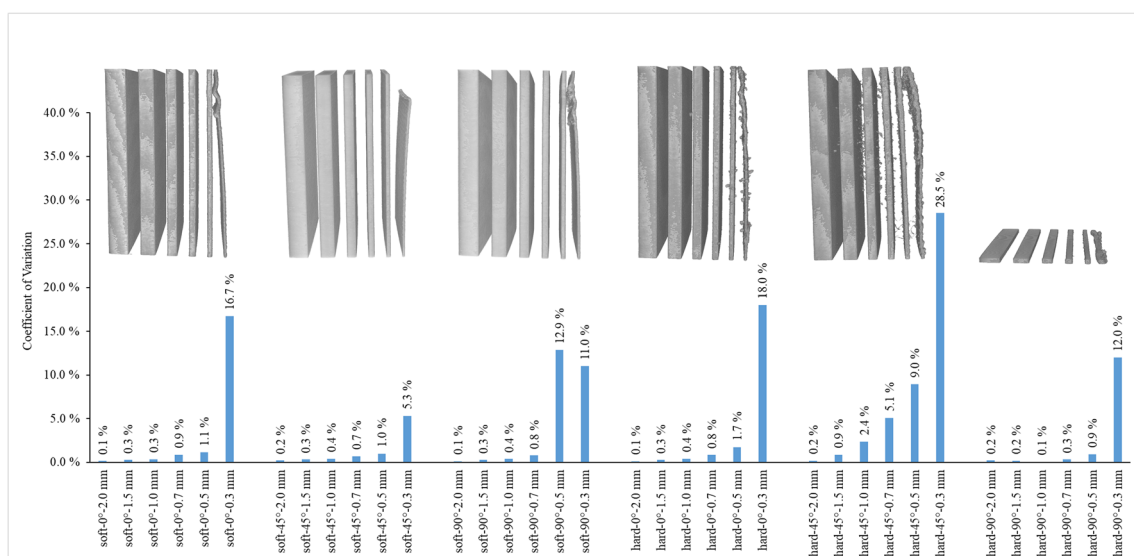


Fig. 8 Coefficient of variation in the cross-sectional area of the thin walls as a function of wall thickness, part orientation and re-coater blade

orientation could not be built for more than ~ 15 layers before build failure). This is also the case for the surface roughness, where it can be seen that the walls built using the soft re-coater blade have smoother surfaces than in the ones built using hard re-coater blade.

When building the overhang specimens horizontally in relation to the re-coating direction with the hard re-coater blade, the features could be built only for ~ 30 layers before fatal collision between the part and re-coater. Therefore, a meaningful comparison about the accuracy of the overhang features could be done only for the overhangs produced in parallel orientation. In this orientation using the hard re-coater blade, the overhangs could be built for ~ 100 layers before the process had to be paused, and the part in question discontinued, due to impact that risked breaking the re-coater. With the soft re-coater, in both orientations the features could be built for the full height (470 layers for the overhang inclined the least, i.e. 45°). However, the geometrical accuracy of the features started to deteriorate earlier. Figure 9 shows the reconstructed 3D volume from the CT scan for the overhang specimens produced both with the soft and hard re-coater. Views from top and bottom surfaces of the overhangs are included. From the top surface, the

length of the overhang feature where it was still properly built was measured. The soft blade resulted in better top surface appearance for a longer feature distance at 45° (7.5 mm vs. 4.1 mm) and 40° (4.9 mm vs 4.5 mm) overhangs. For the steeper overhangs of 35°, 30° and 25° degrees, the hard re-coater blade was able to produce the features for 25%, 128%, and 168% longer distances, respectively, before severe deformation starts. It can be further seen that the bottom surface quality also deteriorates to a higher degree when using the soft re-coater blade.

3.3 Porosity

Table 1 shows the total porosity in the volume as calculated separately for each feature (thin walls and the solid bottom) using the method described in Sect. 2. First, it can be seen that when building bulk material (13 × 15 × 6 mm solid bottom in this case), the porosities remain extremely low (≤ 0.001%) with barely any noticeable defects with the 11 μm resolution of the CT scan in all the specimens, regardless of part orientation or re-coater blade. It is interesting to note that the spatters remaining on the 13 × 15 mm surface when using soft re-coater blade (see Fig. 6a) did not result in

Fig. 9 Top and bottom surface qualities of the overhang features produced with the soft (left) and hard (right) blade. From the top surface, the length of the overhang properly produced is measured for quantitative comparison

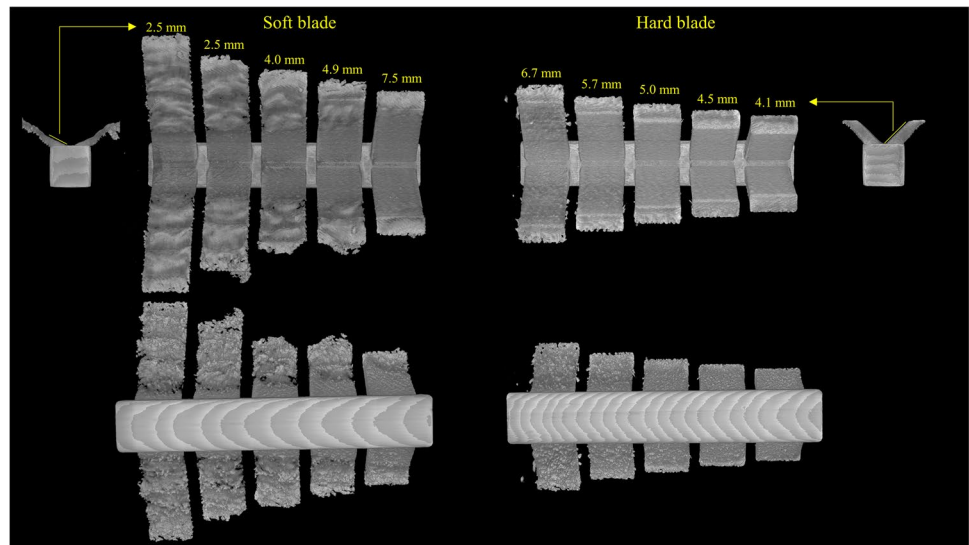


Table 1 The overall porosity of each feature in the thin-walled specimens as a function of wall thickness, part orientation and re-coater blade

	Soft blade			Hard blade		
	0°	45°	90°	0°	45°	90°
Solid bottom	0.001%	0.001%	0.000%	0.001%	0.000%	0.001%
2.0-mm wall	0.000%	0.000%	0.000%	0.000%	0.000%	0.002%
1.5-mm wall	0.001%	0.000%	0.000%	0.001%	0.004%	0.014%
1.0-mm wall	0.001%	0.000%	0.000%	0.001%	0.010%	0.027%
0.7-mm wall	0.004%	0.008%	0.164%	0.002%	0.034%	0.512%
0.5-mm wall	0.125%	0.288%	0.501%	0.054%	0.390%	1.484%
0.3-mm wall	0.434%	1.232%	0.458%	0.927%	1.722%	2.345%

increased porosity. However, when building the thin walls, differences start to emerge. When the wall thickness is considerable (> 1.0 mm in this case), porosities remain comparable to the extremely low levels of bulk material. When the wall thickness is reduced below this, porosity increases exponentially. At these thin features, differences emerge between the part orientations and the used re-coater blade. Overall, lowest porosities in all the studied conditions are achieved when building with soft re-coater blade and the walls oriented parallel (0°) to the re-coating direction. On the other hand, highest overall porosities are observed when building with the hard blade the walls oriented horizontally (90°) to the re-coating direction. When comparing the soft/hard re-coater to each other per part orientation, it can be seen that the use of soft re-coater resulted in less porosity for the thinnest 0.3-mm walls. However, for the 0.5-mm and 0.7-mm wall thicknesses, it can be seen that the hard re-coater resulted in lower porosity in 0° part orientation. On the other hand, in part orientations 45° and 90° , the use of soft blade resulted in less porosity also for the 0.5-mm and 0.7-mm wall thicknesses. The largest difference in porosity between same wall thickness and part orientation was with

0.3-mm wall at 90° orientation. In this condition, the hard re-coater blade resulted in 412% higher porosity than the soft blade. This highlights the importance of studying the effect of using hard/soft re-coater blade on the porosity in the context of the part orientation, as this is also a significant factor. Furthermore, if the comparison would be only made building bulk features such as simple cubes or cylinders, no difference would be observed in the resulting porosity as both re-coating blades perform as well as the other in such scenarios. When building complex features (which is the case most often in real-life additive manufacturing applications), the effect of the re-coater blade becomes significant.

In Fig. 10, the number of defects as a function of wall thickness, part orientation and re-coater blade is shown. Note that the walls for the 90° specimen with the hard blade could be only built up to ~ 15 layers; hence, the sample size for the defect distribution was much smaller here than in the others; nevertheless, it was included for comparison. To allow for the comparison, the defect count was normalized per number of layers built for each specimen. Multiple observations can be made from the defect distributions. First, it can be seen that in all cases, most defects are generated within the

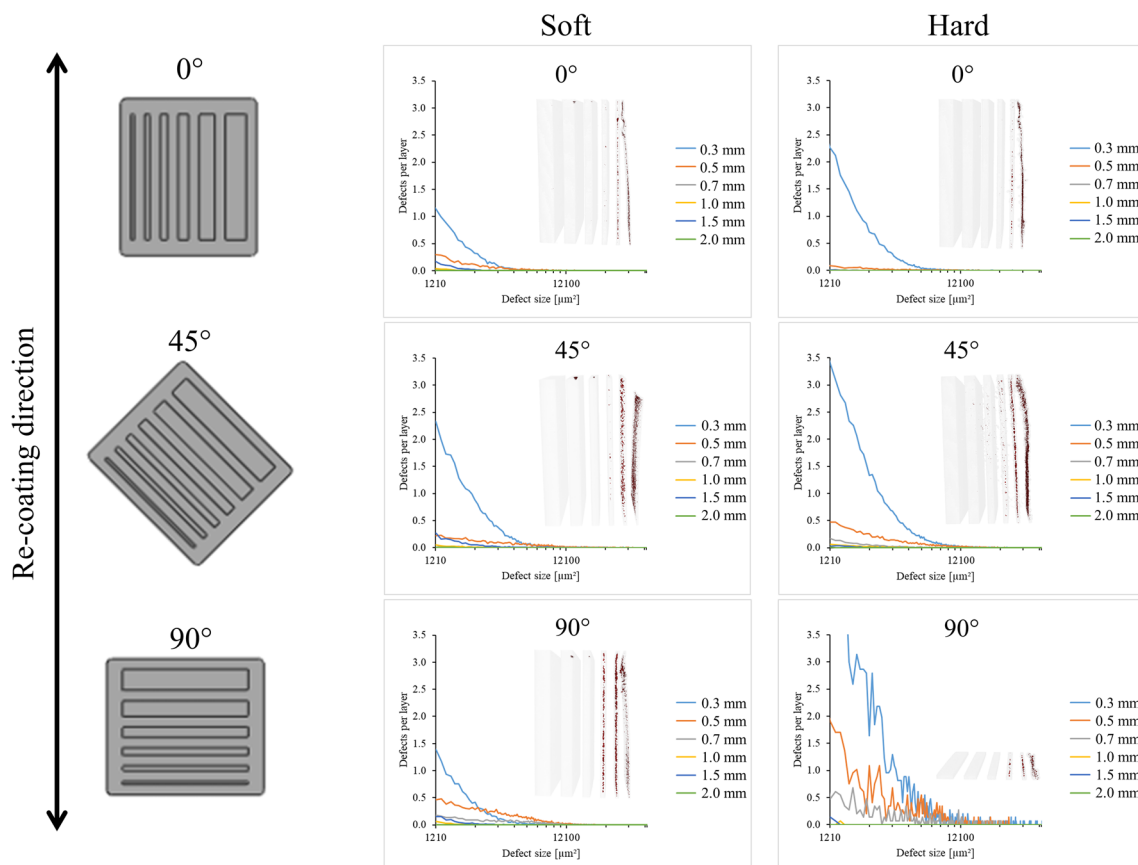


Fig. 10 Number of defects per layer larger than 10 pixel ($1210 \mu\text{m}^2$) as a function of wall thickness, part orientation and re-coater blade. Note the logarithmic scale on x-axis

thinnest 0.3-mm wall. In all three-part orientations, the hard blade resulted in more defects in the 0.3-mm wall. However, in orientation 0° when the walls are built along the re-coating direction, the walls > 0.3 mm had more defects when built with the soft re-coater blade than with the hard blade. On the contrary, when the part orientation is 45° or 90° in relation to the re-coater, the hard re-coater blade results in more defects also in the walls > 0.3 mm. This is caused by impacts with the re-coater in these part orientations. When the thinnest 0.3-mm wall is in an angle (45°, 90° in this study) in relation to the re-coater, the hard blade bends the thin wall causing it to vibrate and disturb the powder bed close to it, as can be seen in Fig. 7. Figure 11 further shows a schematic illustration of powder blown away from around the 0.3-mm wall and re-distributed on top of all the features of the part. This essentially leads to uneven effective powder layer thickness on these locations for the next layer. As the laser energy remains constant, a smaller effective layer thickness could lead to keyhole porosity, whereas an increased effective layer thickness would cause increased risk for lack of fusion porosity. This shows as overall increased number

of defects when building the thin walls with the hard blade, as quantified in Fig. 10.

Figure 12 shows the size distributions of internal defects from the overhangs produced using either a soft or hard re-coater blade. As the overhangs oriented perpendicular to the re-coating direction could be built only for ~ 30 layers with hard re-coater, a meaningful comparison could be only made for the overhangs built in along the re-coating direction. As could be expected, for both re-coater blades the number of defects increases when the overhang inclination angle decreases. Using the hard blade resulted in smaller and overall less defects on the overhangs. The average defect diameter was calculated assuming spherical defect shape. Depending on the overhang angle, with soft blade the defects had 1.3–2.0 times larger diameters than with hard blade. The difference observed between the blades is most likely due to at least two reasons. First, the damage caused by the deformed overhangs to the soft re-coater blade results in uneven powder layer thicknesses on the subsequent layers, which leads to defects via similar mechanism as illustrated in Fig. 6c. On the contrary, a

Fig. 11 Schematic illustration of the contact between a feature rising from the powder bed and the hard re-coater blade, causing the deformation and vibration of the thin feature, leading to locally uneven powder layer thicknesses on top of the part and eventually to increased internal defects

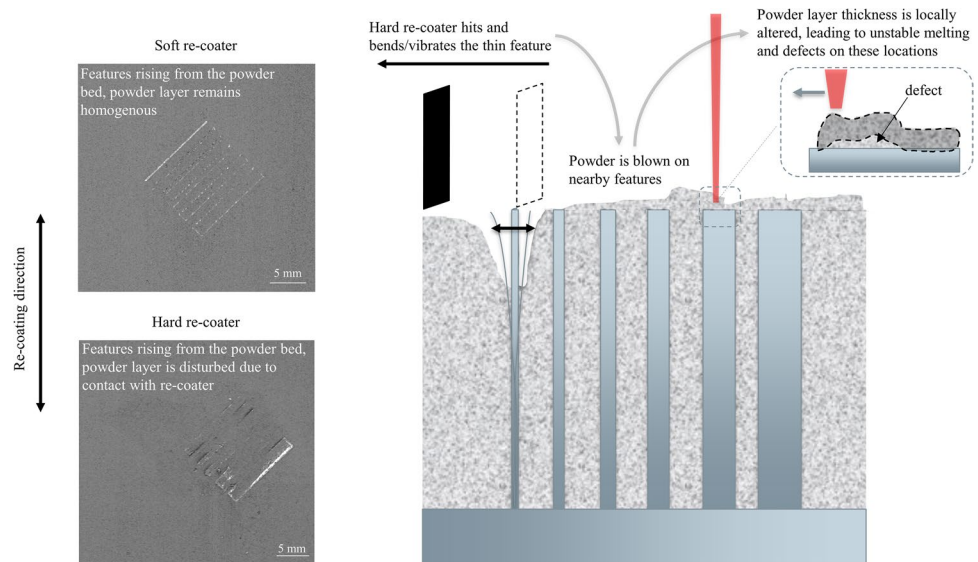
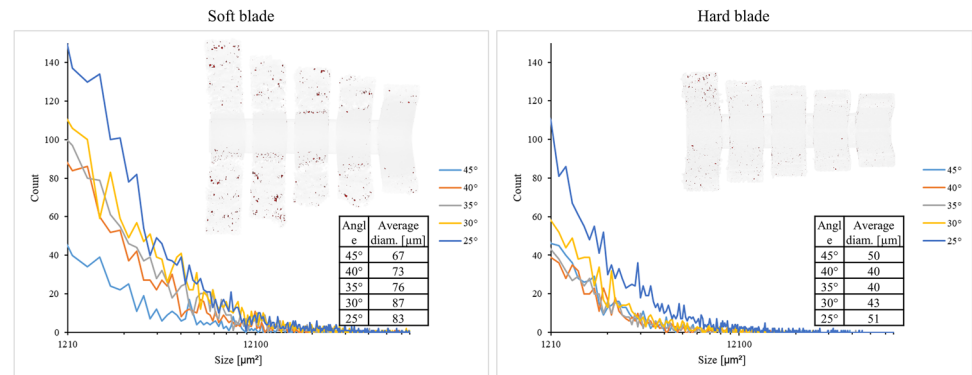


Fig. 12 Number of defects larger than 10 pixel (1210 μm²) as a function of overhang inclination angle and re-coater blade. Average diameter (assuming spherical defect shape) of each distribution is included. Note the logarithmic scale on x-axis



similar collision with the hard re-coater leads to interruption of the build cycle as explained in Sect. 3.1. Second, as with the soft blade the build cycle is not interrupted even as the overhangs are heavily deformed, the poor down-facing surface leads to burn through, sintering of unmelted powder particles to the down-facing surface and increase in defects. With the hard re-coater, the severe deformation of the overhangs causes the build cycle to stop all together in similar situation. However, up until that point of failure, the number of defects remains lower than with the soft blade.

From the results when building the overhangs with either hard or a soft blade, a trade-off between part quality and processability can be identified. With the soft re-coater blade, steep overhangs can be built to a longer distance without interruption to the build cycle but with low surface quality, geometrical accuracy and high number of internal defects, whereas with the hard re-coater blade the quality remains higher to a certain extent, after which a terminal collision between the deformed feature and hard re-coater causes the build cycle to cease all together. With the thin walls, indications of a similar effect can be observed; however, another phenomenon, namely the disturbances caused to the powder bed by the thin wall vibrating after a contact with the hard blade, further decreased the quality when processing with the hard blade. This resulted in a situation where the soft blade performed better both in terms of processability and the lower number of internal defects in the case of the thin walls. It is acknowledged, however, that the situation may be different, if the thin walls would be produced further apart from one another. Then, the disturbances caused by the 0.3-mm wall would not cause defects to the other walls. Similarly, if the overhangs would be processed separately and not attached to the same single bottom piece, it may be that the least inclined overhangs of 40 and 45° could be properly produced even further than seen in Fig. 9 for the hard blade. Both scenarios are relevant and come across in real-world applications when producing parts with PBF-LB, so the choice of the re-coater blade (hard or soft) should be made case-by-case for each type of component geometry. Furthermore, it is acknowledged that the re-coating sledge of the SLM 125 used in this study is attached firmly from both ends and is quite rigid. Some PBF-LB systems use re-coating arms that are attached on only one end and the other end is free. Further studies should be conducted to see whether similar results would be attained with machines having less rigid re-coater arms, as this could have an effect on how the re-coater blade behaves during an impact with a feature rising from the powder bed. Also, the effect of different re-coating speeds on the severity of powder bed disturbances upon impact with such features could be studied.

4 Conclusions

From the presented results, the following conclusions can be drawn. When building bulk material without any complex features, both the hard and soft re-coating blade results in extremely low porosity $\leq 0.001\%$ without any issues in the processability. However, when building thin walls, especially those below a thickness of 1.0 mm, differences emerge. Contact with the hard re-coater blade and a thin feature led to severe disturbances in the powder bed, causing the effective layer thickness to change locally in the powder bed. This leads to uneven melting conditions in these locations, resulting in increased porosity. This effect is most pronounced, when the features are built in an angle in relation to the re-coating direction. A similar contact with the soft re-coater blade does not lead to such disturbances to the powder bed, ultimately leading to less porosity formation through this phenomenon. It was shown here that this phenomenon can be automatically identified and quantified from the powder bed images acquired with a contact image sensor utilizing the short focal distance of the sensor, which could be utilized as a quality control method.

With some challenging features (such as the thin walls oriented horizontally and the studied overhangs), the unyielding hard blade results in such severe impact with the part from which the features have risen above the powder bed, that there was risk of severe failure of the whole re-coating mechanism, and the build cycle was paused and the part in question had to be discontinued. On the contrary, in the same situation the soft blade would yield, allowing for the build cycle to continue and the part to finish, but resulting in damage to the re-coater blade and hence uneven powder spreading for the subsequent layers. With steep overhangs, even as the part could be finished with the soft blade, the geometrical accuracy and surface finish were reduced and the number of internal defects increased compared to the overhangs built with the hard re-coater blade.

This study highlighted the need to analyze the effect of PBF-LB processing parameters, such as the re-coater blade type, on final part properties having challenging geometrical features, which are typical for PBF-LB AM parts in real-world applications, instead of relying just on measurements made from simple cube or cylinder specimens in such applications where intricate features are present. Finally, as the re-coater blade was shown to have significant effect on the quality of parts containing features such as thin walls and overhangs, it is recommended that the re-coater blade type is included as an essential parameter in PBF-LB process qualification and procedure specifications in such cases.

Acknowledgements The authors would like to thank Kimmo Ruusu- vuori from VTT for operating the PBF system. We thank Jukka Kuva

from GTK for CT scanning, which is supported by the Academy of Finland via RAMI infrastructure project (#293109).

Author contribution J. R.: conceptualization, methodology, formal analysis, investigation, writing—original draft, writing—review and editing, visualization. A. R.: methodology, investigation, software, writing—original draft, writing—review and editing, visualization. S. M–K.: conceptualization, resources, writing—review and editing, supervision, funding acquisition. A. S.: writing—review and editing, supervision.

Funding Open Access funding provided by Technical Research Centre of Finland. This work was supported by VTT Technical Research Centre of Finland (project numbers 132261, 132610 and 132607). J.R. is grateful to Walter Ahlström Foundation (Grant number 20230045) for supporting this work.

Data availability The raw data required to reproduce the findings of this work are available from the corresponding author upon reasonable request.

Declarations

Competing interests The authors declare no competing interests.

Open Access This article is licensed under a Creative Commons Attribution 4.0 International License, which permits use, sharing, adaptation, distribution and reproduction in any medium or format, as long as you give appropriate credit to the original author(s) and the source, provide a link to the Creative Commons licence, and indicate if changes were made. The images or other third party material in this article are included in the article's Creative Commons licence, unless indicated otherwise in a credit line to the material. If material is not included in the article's Creative Commons licence and your intended use is not permitted by statutory regulation or exceeds the permitted use, you will need to obtain permission directly from the copyright holder. To view a copy of this licence, visit <http://creativecommons.org/licenses/by/4.0/>.

References

- Capozzi LC, Sivo A, Bassini E (2022) Powder spreading and spreadability in the additive manufacturing of metallic materials: a critical review. *J Mater Process Technol* 308:117706. <https://doi.org/10.1016/j.jmatprotec.2022.117706>
- Nayak SK, Jinoop AN, Paul CP et al (2022) On the hot isostatic pressing of Inconel 625 structures built using laser powder bed fusion at higher layer thickness. *Int J Adv Manuf Technol* 120:4065–4078. <https://doi.org/10.1007/s00170-022-08960-4>
- Greco S, Gutzeit K, Hotz H et al (2020) Selective laser melting (SLM) of AISI 316L—impact of laser power, layer thickness, and hatch spacing on roughness, density, and microhardness at constant input energy density. *Int J Adv Manuf Technol* 108:1551–1562. <https://doi.org/10.1007/s00170-020-05510-8>
- Leicht A, Fischer M, Klement U et al (2021) Increasing the productivity of laser powder bed fusion for stainless Steel 316L through increased layer thickness. *J Mater Eng Perform* 30:575–584. <https://doi.org/10.1007/s11665-020-05334-3>
- Fox H, Kamaraj AB, Drake D (2022) Investigating the effect of powder recoater blade material on the mechanical properties of parts manufactured using a powder-bed fusion process. *Manuf Lett* 00:561–568. <https://doi.org/10.1016/j.mfglet.2022.07.071>
- Jacob G, Donmez A, Slotwinski J, Moylan S (2016) Measurement of powder bed density in powder bed fusion additive manufacturing processes. *Meas Sci Technol* 27:115601. <https://doi.org/10.1088/0957-0233/27/11/115601>
- Choi JP, Shin GH, Lee HS et al (2017) Evaluation of powder layer density for the selective laser melting (SLM) process. *Mater Trans* 58:294–297. <https://doi.org/10.2320/matertrans.M2016364>
- Wischeropp TM, Emmelmann C, Brandt M, Pateras A (2019) Measurement of actual powder layer height and packing density in a single layer in selective laser melting. *Addit Manuf* 28:176–183. <https://doi.org/10.1016/j.addma.2019.04.019>
- Oropeza D, Penny RW, Gilbert D, Hart AJ (2022) Mechanized spreading of ceramic powder layers for additive manufacturing characterized by transmission x-ray imaging: influence of powder feedstock and spreading parameters on powder layer density. *Powder Technol* 398:117053. <https://doi.org/10.1016/j.powtec.2021.117053>
- Marchais K, Girardot J, Metton C, Iordanoff I (2021) A 3D DEM simulation to study the influence of material and process parameters on spreading of metallic powder in additive manufacturing. *Comput Part Mech*. <https://doi.org/10.1007/s40571-020-00380-z>
- Shaheen MY, Thornton AR, Luding S, Weinhart T (2021) The influence of material and process parameters on powder spreading in additive manufacturing. *Powder Technol* 383:564–583. <https://doi.org/10.1016/j.powtec.2021.01.058>
- Haeri S (2017) Optimisation of blade type spreaders for powder bed preparation in Additive Manufacturing using DEM simulations. *Powder Technol* 321:94–104. <https://doi.org/10.1016/j.powtec.2017.08.011>
- Wang L, Yu A, Li E et al (2021) Effects of spreader geometry on powder spreading process in powder bed additive manufacturing. *Powder Technol* 384:211–222. <https://doi.org/10.1016/j.powtec.2021.02.022>
- Li E, Zhou Z, Wang L et al (2022) Particle scale modelling of powder recoating and melt pool dynamics in laser powder bed fusion additive manufacturing: a review. *Powder Technol* 409:117789. <https://doi.org/10.1016/j.powtec.2022.117789>
- Oropeza D, Roberts R, Hart AJ (2021) A modular testbed for mechanized spreading of powder layers for additive manufacturing. *Rev Sci Instrum* 92:015114. <https://doi.org/10.1063/5.0031191>
- Hulme CN, Mellin P, Marchetti L et al (2022) A practicable and reliable test for metal powder spreadability: development of test and analysis technique. *Prog Addit Manuf*. <https://doi.org/10.1007/s40964-022-00341-3>
- Snow Z, Martukanitz R, Joshi S (2019) On the development of powder spreadability metrics and feedstock requirements for powder bed fusion additive manufacturing. *Addit Manuf* 28:78–86. <https://doi.org/10.1016/j.addma.2019.04.017>
- Yuasa K, Tagami M, Yonehara M et al (2021) Influences of powder characteristics and recoating conditions on surface morphology of powder bed in metal additive manufacturing. *Int J Adv Manuf Technol* 115:3919–3932. <https://doi.org/10.1007/s00170-021-07359-x>
- Daña M, Zetková I, Hanzl P (2019) The influence of a ceramic recoater blade on 3D printing using direct metal laser sintering. *Manuf Technol* 19:23–28. <https://doi.org/10.21062/ujep/239.2019/a/1213-2489/mt/19/1/23>
- Shamsdini SAR, Ghoncheh MH, Mohammadi M (2021) Effect of recoater-blade type on the mechanical properties and microstructure of additively manufactured maraging steels. *Mater Sci Eng A* 812:141104. <https://doi.org/10.1016/j.msea.2021.141104>
- Zhang M, Sun CN, Zhang X et al (2018) Elucidating the relations between monotonic and fatigue properties of laser powder bed fusion stainless steel 316L. *Jom* 70:390–395. <https://doi.org/10.1007/s11837-017-2640-z>
- Abdelrahman M, Reutzel EW, Nassar AR, Starr TL (2017) Flaw detection in powder bed fusion using optical imaging. *Addit Manuf* 15:1–11. <https://doi.org/10.1016/j.addma.2017.02.001>

23. Lu QY, Nguyen NV, Hum AJW et al (2019) Optical in-situ monitoring and correlation of density and mechanical properties of stainless steel parts produced by selective laser melting process based on varied energy density. *J Mater Process Technol* 271:520–531. <https://doi.org/10.1016/j.jmatprotec.2019.04.026>
24. Barrett C, MacDonald E, Conner B, Persi F (2018) Micron-level layer-wise surface profilometry to detect porosity defects in powder bed fusion of Inconel 718. *Jom* 70:1844–1852. <https://doi.org/10.1007/s11837-018-3025-7>
25. Fleming TG, Nestor SGL, Allen TR et al (2020) Tracking and controlling the morphology evolution of 3D powder-bed fusion in situ using inline coherent imaging. *Addit Manuf* 32:100978. <https://doi.org/10.1016/j.addma.2019.100978>
26. Fischer FG, Birk N, Rooney L et al (2021) Optical process monitoring in Laser Powder Bed Fusion using a recoater-based line camera. *Addit Manuf* 47:102218. <https://doi.org/10.1016/j.addma.2021.102218>
27. Fischer FG, Zimmermann MG, Praetzs N, Knaak C (2022) Monitoring of the powder bed quality in metal additive manufacturing using deep transfer learning. *Mater Des* 222:111029. <https://doi.org/10.1016/j.matdes.2022.111029>
28. Pedersen DB, Eiriksson ER, Aanaes H, Hansen HN (2016) In-situ monitoring in additive manufacturing using contact image sensors. In: *Proceedings of the ASPE/euspen 2016 Summer Topical Meeting on Dimensional Accuracy and Surface Finish in Additive Manufacturing*. ASPE – The American Society for Precision Engineering, ASPE Summer Topical Meeting 2016. ASPE, Raleigh, United States, pp 114–118
29. Tan Phuc L, Seita M (2019) A high-resolution and large field-of-view scanner for in-line characterization of powder bed defects during additive manufacturing. *Mater Des* 164:107562. <https://doi.org/10.1016/j.matdes.2018.107562>
30. Le T-P, Wang X, Davidson KP et al (2021) Experimental analysis of powder layer quality as a function of feedstock and recoating strategies. *Addit Manuf* 39:101890. <https://doi.org/10.1016/j.addma.2021.101890>
31. Lu Q, Grasso M, Le TP, Seita M (2022) Predicting build density in L-PBF through in-situ analysis of surface topography using powder bed scanner technology. *Addit Manuf* 51:102626. <https://doi.org/10.1016/j.addma.2022.102626>
32. Bugatti M, Colosimo BM (2022) The intelligent recoater: a new solution for in-situ monitoring of geometric and surface defects in powder bed fusion. *Addit Manuf Lett* 3:100048. <https://doi.org/10.1016/j.addlet.2022.100048>
33. Yang H, Reijonen J, Revuelta A (2023) Multi-resolution Quality Inspection of Layerwise Builds for Metal 3D Printer-and-Scanner. *J Manuf Sci Eng* 145(10):101004. <https://doi.org/10.1115/1.4057013>
34. Ahmed A, Majeed A, Atta Z, Jia G (2019) Dimensional quality and distortion analysis of thin-walled alloy parts of AlSi10Mg manufactured by selective laser melting. *J Manuf Mater Process* 3(2):51. <https://doi.org/10.3390/jmmp3020051>

Publisher's Note Springer Nature remains neutral with regard to jurisdictional claims in published maps and institutional affiliations.